Rapid Communications | Editors' Suggestion

Emergent dual topology in the three-dimensional Kane-Mele Pt_2HgSe_3

Antimo Marrazzo,[1] Nicola Marzari,[1] and Marco Gibertini[2]

[1]*Theory and Simulation of Materials (THEOS), and National Centre for Computational Design and Discovery of Novel Materials (MARVEL), École Polytechnique Fédérale de Lausanne, CH-1015 Lausanne, Switzerland*

[2]*Department of Quantum Matter Physics, University of Geneva, 24 Quai Ernest Ansermet, CH-1211 Geneva, Switzerland*

(Received 13 September 2019; accepted 6 February 2020; published 13 March 2020)

Recently, the very first large-gap Kane-Mele quantum spin Hall insulator was predicted to be monolayer jacutingaite (Pt_2HgSe_3), a naturally occurring exfoliable mineral discovered in Brazil in 2008. The stacking of quantum spin Hall monolayers into a van-der-Waals layered crystal typically leads to a (0;001) weak topological phase, which does not protect the existence of surface states on the (001) surface. Unexpectedly, recent angle-resolved photoemission spectroscopy experiments revealed the presence of surface states dispersing over large areas of the 001-surface Brillouin zone of jacutingaite single crystals. The 001-surface states have been shown to be topologically protected by a mirror Chern number $C_M = -2$, associated with a nodal line gapped by spin-orbit interactions. Here, we extend the two-dimensional Kane-Mele model to bulk jacutingaite and unveil the microscopic origin of the gapped nodal line and the emerging crystalline topological order. By using maximally localized Wannier functions, we identify a large nontrivial second nearest-layer hopping term that breaks the standard paradigm of weak topological insulators. Complemented by this term, the predictions of the Kane-Mele model are in remarkable agreement with recent experiments and first-principles simulations, providing an appealing conceptual framework also relevant for other layered materials made of stacked honeycomb lattices.

DOI: 10.1103/PhysRevResearch.2.012063

Graphene crystal and electronic structure has been fundamental for the development of the theory of topological insulators (TIs). The very first model of a TI ever proposed, namely the Chern (or quantum anomalous Hall) insulator by Haldane, is essentially a two-band tight-binding model for graphene in the presence of a staggered magnetic field [1]. The experimental isolation of graphene [2] inspired Kane and Mele to assert that by doubling Haldane's model and introducing spins one could describe intrinsic spin-orbit coupling (SOC) in graphene, leading to a novel gapped topological phase [3,4]. Such phase, identified by a $\mathbb{Z}_2$ topological invariant, is named quantum spin Hall insulator (QSHI) and it is protected by time-reversal symmetry. Nowadays, graphene and the Kane-Mele (KM) model stand as one of the archetypal time-reversal invariant TIs, although negligible relativistic effects in carbon open only a vanishingly small band gap in graphene [5].

Notably, the KM model still applies to all Xenes [6], i.e., the two-dimensional (2D) unary honeycomb materials made of group IV elements (e.g., silicene, germanene, and stanene), where the presence of heavier atoms should lead to sizable band gaps [6–8]. Recently, monolayers of jacutingaite (Pt_2HgSe_3) have also been proposed as novel QSHIs that display the KM physics, and at a much larger energy scale than in Xenes, with a band gap estimated to be around ∼0.5 eV [9]. Jacutingaite is a naturally occurring layered mineral first discovered in 2008 [10] in a Brazilian mine and then synthesized in 2012 [11]. Although jacutingaite is a ternary material with several differences with respect to the Xenes, it shares a (buckled) honeycomb structure of mercury atoms [see Fig. 1(a)], which is ultimately responsible for the KM physics in monolayers [9] that sparked experimental [12–14] and theoretical [14–17] interest in this material.

Being a stack of 2D QSHIs, bulk jacutingaite is expected to be a 3D weak TI with indices (0; 001), and thus with no surface states on the (001) surface [18]. Recent first-principles simulations confirmed this weak topological classification [14–16], but at the same time surprisingly predicted the presence of basal surface states associated with a nontrivial mirror Chern number C_M, thus promoting bulk jacutingaite to a dual topological material [19,20] with both weak and crystalline topological properties. Such (001) surface states have now been demonstrated independently through angle-resolved photoemission spectroscopy (ARPES) experiments on synthetic jacutingaite single crystals [14]. The unexpected dual topology of bulk jacutingaite cannot be understood through the standard paradigm of weak TIs [18] and its interpretation opens interesting perspectives on nontrivial extensions of the KM model to describe 3D stacks of honeycomb layers.

Here we show that the nontrivial topology in bulk jacutingaite emerges from a strong interlayer hybridization that leads to a 3D generalization of the KM model including a large peculiar *second nearest-layer hopping* term, while nearest layers are almost decoupled. Within this picture, even and odd layers are approximately independent and can be separately described by a 3D KM model where the novel hopping term drives a band inversion, giving rise to a nodal

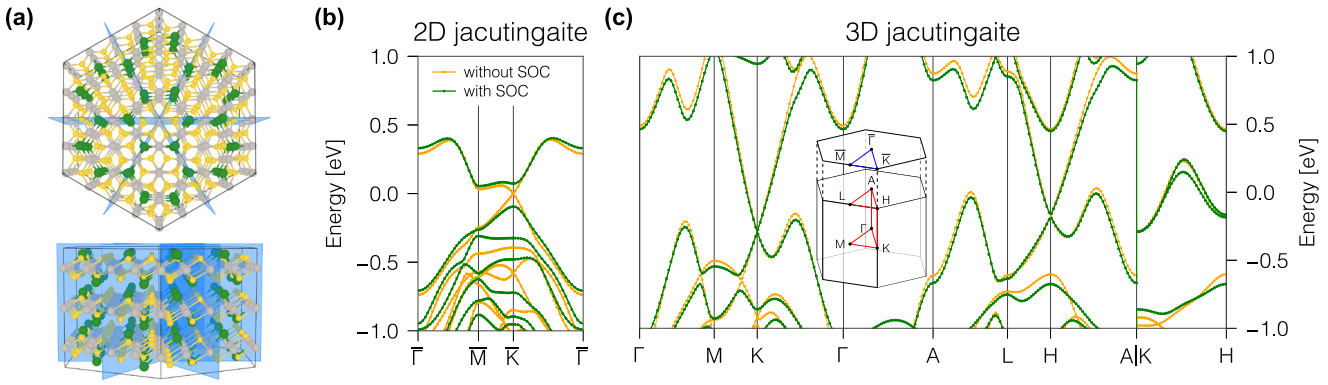

FIG. 1. (a) Top and lateral views of jacutingaite crystal structure, where the threefold symmetric mirror planes are highlighted in blue. Mercury, platinum, and selenium atoms are represented in green, grey, and yellow, respectively. [(b) and (c)] Band structure of monolayer (b) and bulk (c) jacutingaite obtained using DFT with (green) and without (orange) SOC. The inset shows the bulk and surface Brillouin zone.

line that is gapped by SOC and a nonzero C_M. Remarkably, when a coupling between even and odd layers is restored, the Chern numbers add up to a nontrivial value while the $\mathbb{Z}_2$ classification becomes weak, thus providing a microscopic understanding for the emergent dual topology of this material.

We first shortly review the band structure of monolayer Pt_2HgSe_3 [shown in Fig. 1(b)] and its relation to the KM model. When SOC is neglected, the valence and conduction bands form Dirac cones located at the corners $\overline{K}/\overline{K}'$ of the 2D Brillouin zone (BZ). In a basis of maximally localized Wannier functions (MLWFs) [21] centered on mercury atoms [9], the linear dispersions arise from a hopping term between nearest neighbors (NNs) on the (buckled) honeycomb Hg (sub)lattice, similarly to graphene. The inclusion of SOC opens a substantial gap (0.15 eV with density-functional theory and ∼0.5 eV at the G_0W_0 level), turning the system into a QSHI. The gap mainly stems from a complex-valued second-nearest-neighbor (second-NN) hopping [9], exactly as proposed by Kane and Mele, so that all qualitative features of the band structure can be understood in terms of the KM model [3,4,22]:

$$H_{KM} = -t \sum_{\langle ij\rangle\alpha} c^{\dagger}_{i\alpha} c_{j\alpha} + i\Delta \sum_{\langle\langle ij\rangle\rangle\alpha\beta} v_{ij} s^{z}_{\alpha\beta} c^{\dagger}_{i\alpha} c_{j\beta} + i\Delta' \sum_{\langle\langle ij\rangle\rangle\alpha\beta} u_{ij} \left(\boldsymbol{s}\times \boldsymbol{d}^{0}_{ij}\right)^{z}_{\alpha\beta} c^{\dagger}_{i\alpha} c_{j\beta}, \quad (1)$$

where the sums are restricted to pairs $\langle ij\rangle$ ($\langle\langle ij\rangle\rangle$) of first- (second-) nearest-neighbor sites i and j, v_{ij}, u_{ij}, and $\boldsymbol{d}^0_{ij}$ are geometrical parameters [23], and $\boldsymbol{s} = (s^x, s^y, s^z)$ are spin Pauli matrices. Here, in addition to the original KM hopping amplitudes t and Δ associated respectively with the NN hopping and the KM SOC, we are adding a second-NN "in-plane" SOC term with amplitude Δ', which is not present in planar honeycomb lattices such as graphene, but that appears when horizontal mirror symmetry is broken [22] as in this case.

Extending naively the analogy between graphene KM model and monolayer jacutingaite to 3D, one would expect the electronic properties of bulk jacutingaite to be almost identical to its 2D form, as in the case of graphene and graphite. In Fig. 1(c), we report the band structure of bulk jacutingaite computed along a high-symmetry path by density-functional theory (DFT) [24]. Without SOC, a linear dispersion is observed close to the K and H points, which is indeed reminiscent of the 2D Dirac cones. Still, the linear behavior extends over a much larger energy range than in 2D and a remarkable energy dispersion appears along the vertical direction between H and K. Even more compelling, SOC opens a gap between valence and conduction bands at K (and H) as in 2D, but the magnitude of the splitting is 1–2 orders of magnitude smaller. Overall, these features suggest a significant coupling between layers, which is consistent with the non-negligible interlayer binding energy reported in Refs. [9,25] that sets jacutingaite as "potentially exfoliable" [25].

To show that this significant interlayer coupling is responsible for the unexpected bulk dual topology, we first develop a minimal tight-binding model that captures all the relevant physics by extracting the most important hopping terms from the complexity of the full electronic structure. We first build a four-band model (including spin) using Hg-centered MLWFs that reproduces the main features of the band structure around the Fermi level [24]. The corresponding Wannier functions are plotted in Fig. 2(a): they clearly resemble the ones obtained for the monolayer in Ref. [9], but a notable difference is due to the spatial extension of the MLWFs; those of bulk jacutingaite spread over a neighboring layer, so that they are effectively localized on two layers.

The strongest hopping term in the MLWF Hamiltonian is the intralayer NN hopping t that is responsible for the linear dispersion close to K and H, with a small gap opened by a very weak KM SOC. The fact that for bulk jacutingaite the effective KM and in-plane SOC are strongly renormalized with respect to the monolayer can be understood by looking at the geometry of the MLWFs. Indeed, as shown in Fig. 2(a), in bulk Pt_2HgSe_3 the overlap between MLWFs allows two alternative paths to hop to second-NNs within the same layer: one identical to monolayer jacutingaite (solid line) and one extending through the closest layer (dashed line). Owing to the different sign of the geometrical parameter v_{ij} (and u_{ij}) in Eq. (1), the two paths give opposite contributions and, being very similar in magnitude, result in a very weak KM (and in-plane) SOC compared to the monolayer.

Remarkably, the second strongest hopping term connects MLWFs localized in *second-nearest layers* as shown in

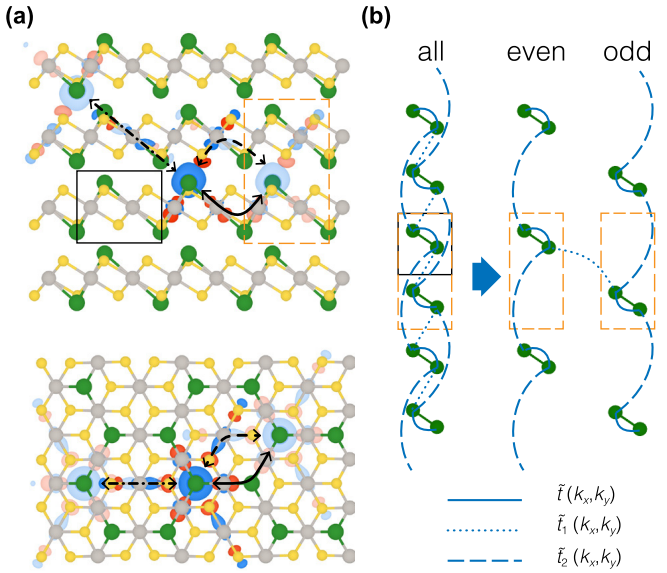

FIG. 2. (a) Lateral and top views of the MLWFs underlying the tight-binding model for bulk jacutingaite. A reference MLWF is shown together with two additional ones (with lighter colors) to highlight the initial and final states of two relevant hopping terms: an intralayer second-nearest-neighbor hopping process (with two possible paths marked with solid or dashed lines) and a second-nearest-layer hopping term (dash-dotted line). (b) Schematic of the effective 1D model describing bulk jacutingaite at fixed parallel momentum $\mathbf{k}_\parallel = (k_x, k_y)$, involving an intralayer $\tilde{t}(\mathbf{k}_\parallel)$, a second-nearest layer $\tilde{t}_2(\mathbf{k}_\parallel)$, and an almost negligible nearest layer $\tilde{t}_1(\mathbf{k}_\parallel)$ hopping term. Even and odd layers are thus almost decoupled and behave as a $\mathbf{k}_\parallel$-dependent Su-Schrieffer-Heeger-like chain with a doubled unit cell (orange dashed line) with respect to the primitive one (black solid line).

Fig. 2(a) (dash-dotted line). Although the MLWFs that are involved are relatively far apart, the large amplitude ($t_2 \simeq -0.7t$) stems from the partial delocalization of the MLWFs over the neighboring layer, which gives rise to a large overlap between MLWF that are two layers apart through the intermediate layer. The strong overlap takes place between a reference MLWF and three others located two layers above (or below) in the opposite sublattice, thus mimicking NN hopping but with a doubled in-plane separation [24].

We now show that this interlayer coupling is crucial for the emergence of the bulk topology by building the following tight-binding model:

$$H_{\mathrm{J3KM}} = H_{\mathrm{KM}} + \lambda \tilde{H}_{2^{\mathrm{nd}}\mathrm{NL}} \tag{2}$$

where H_{KM} is the 2D KM model of Eq. (1), $\tilde{H}_{2^{\mathrm{nd}}\mathrm{NL}}$ is the second nearest-layer hopping just mentioned that makes the model essentially 3D, and λ is a dimensionless coupling constant that interpolates between monolayer ($\lambda = 0$) and bulk ($\lambda = 1$) jacutingaite. This model is a generalization of the Kane-Mele model to 3D jacutingaite and hereafter we will call it J3KM model. As shown in Fig. 2(b), at this level even and odd layers are completely decoupled, so it is natural to choose a unit cell that is doubled along the stacking axis and to describe separately even and odd layers through Eq. (2). In this way, $\tilde{H}_{2^{\mathrm{nd}}\mathrm{NL}}$ becomes a first-nearest layer term in the even/odd subspace, and the BZ is halved along k_z.

We start by considering the J3KM model without SOC, corresponding to an Hamiltonian with only two terms: first nearest-neighbor (as in graphene) and inter-layer hopping. The band structure for a 30-layer slab is reported in Fig. 3(a) for different values of λ, where states localized at the (001) surface are colored in red [27]. For $\lambda = 1$ (bulk jacutingaite), in addition to the graphenelike Dirac states at $\overline{K}$, such simple model accounts for the presence of additional linear crossings between valence and conduction bands (e.g., at a low-symmetry point between $\overline{\Gamma}$ and $\overline{M}$), in perfect agreement with current ARPES measurements [14]. Notably, the model also exhibits 001-surface states that roughly span the same BZ region as observed in experiments [14], thus providing a remarkably realistic qualitative description of the system, despite its simplicity.

An interesting feature of the J3KM model that helps to rationalize the presence of surface states is that, at a given parallel momentum $\mathbf{k}_\parallel = (k_x, k_y)$, it is equivalent to a $\mathbf{k}_\parallel$-dependent 1D tight-binding Hamiltonian analogous to the Su-Schrieffer-Heeger (SSH) one, where the alternating hopping energies, $\tilde{t}(\mathbf{k}_\parallel)$ and $\tilde{t}_2(\mathbf{k}_\parallel)$, depend parametrically on $\mathbf{k}_\parallel$ (see Fig. 2(b) and [24]). The topological properties of this effective 1D chain can be expressed in terms of the Zak phase [28,29]:

$$\gamma(\mathbf{k}_\parallel) = -i \oint \langle u(\mathbf{k}_\parallel, k_z) | \partial_{k_z} u(\mathbf{k}_\parallel, k_z) \rangle dk_z, \tag{3}$$

where $u(\mathbf{k}_\parallel, k_z)$ is the periodic part of the occupied eigenstate. The combination of time-reversal and inversion symmetry dictates that $\gamma(\mathbf{k}_\parallel)$ can only assume two topologically distinct values: $\gamma(\mathbf{k}_\parallel) = \pi$ and $\gamma(\mathbf{k}_\parallel) = 0$, depending on the relative strength of $\tilde{t}(\mathbf{k}_\parallel)$ and $\tilde{t}_2(\mathbf{k}_\parallel)$ as in the SSH model. According to Refs. [30,31], we then expect surface states for all values of $\mathbf{k}_\parallel$ for which $\gamma(\mathbf{k}_\parallel) = \pi$, which is indeed the case in Figs. 3(a) and 3(b).

The analogy with the SSH model also reveals that, along the lines that separate topologically distinct regions of the BZ, we need to have $|\tilde{t}(\mathbf{k}_\parallel)| = |\tilde{t}_2(\mathbf{k}_\parallel)|$, so that the gap closes for some value of k_z. Indeed, by computing the energy bands of the J3KM model without SOC we uncover the presence of a nodal line [see Fig. 3(c)] dispersing across the border of the reduced BZ, also predicted by first-principles simulations [14,16]. Its projection on the (k_x, k_y) plane is consistent with the boundary between regions with topologically distinct Zak phases where $|\tilde{t}(\mathbf{k}_\parallel)| = |\tilde{t}_2(\mathbf{k}_\parallel)|$ [32].

To understand the emergence of surface states and nodal lines, in Figs. 3(a) and 3(b), we show the predictions of the J3KM model as a function of the interlayer coupling λ. For small λ, the band structure is essentially graphenelike, with no surface states and a trivial Zak phase over the full BZ. With increasing λ, a band inversion occurs at the time-reversal-invariant point L of the reduced BZ (corresponding to $\overline{M}$ in 2D), creating three inequivalent nodal lines whose projections separate regions with different Zak phases. Correspondingly, surface states appear in the slab calculation wherever $\gamma(\mathbf{k}_\parallel) = \pi$. With a further increase in λ, the three nodal lines merge into a single one, as shown in Fig. 3(c) for bulk jacutingaite ($\lambda = 1$). The interlayer coupling thus plays a crucial role in driving the expected electronic structure of weakly coupled layers into the rich physics of bulk jacutingaite [38].

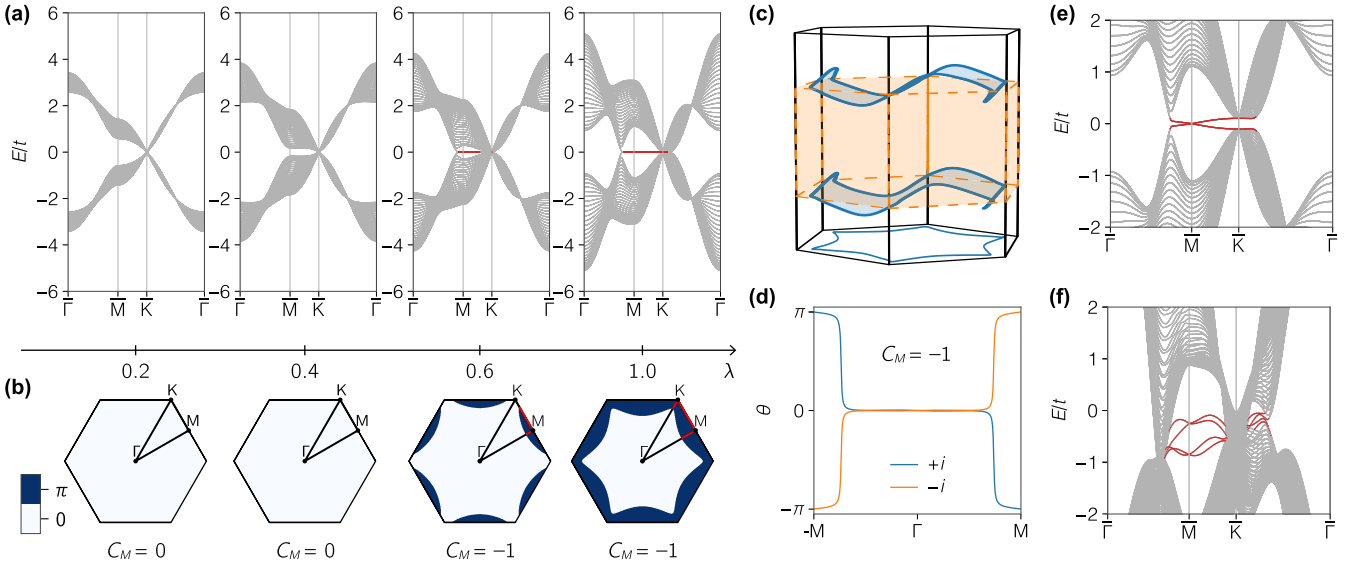

FIG. 3. [(a) and (b)] Evolution of the J3KM model at zero SOC for different values of the interlayer coupling λ in Eq. (2): (a) 30-layer slab band structure, with surface states colored in red and (b) Zak phase (3) over the 2D BZ. (c) Nodal lines in the J3KM model without SOC. The primitive BZ (black solid line) is shown together with the reduced one (orange dashed line) associated with the doubling of the unit cell. [(d) and (e)] J3KM model with SOC: (d) calculation of the mirror Chern number C_M as the winding of the Wilson loop phase θ (restricted to states with a definite $\pm i$ mirror eigenvalue) as a function of the parallel momentum in a mirror-invariant plane [26]. The evolution of C_M with λ is also reported in (b). (e) 30-layer slab band structure as in (a) for $\lambda = 1$ but with SOC included. (f) 60-layer slab band structure for the full MLWF model with SOC. Band energies have been rescaled by the nearest-neighbor hopping amplitude t (=0.27 eV in bulk jacutingaite) by setting the following parameters $t_2/t = -0.7$ and $\Delta/t = \Delta'/t = 0.02$ in Eqs. (1) and (2) [24].

We now include SOC to show the robustness of surface states and their topological protection within the J3KM model. The KM SOC [3,4] gaps the nodal line almost everywhere, but not at the intersections with the vertical mirror-symmetric planes. The inclusion of also the in-plane SOC [6,22] fully gaps the residual Dirac points and the system becomes a topological crystalline insulator, as supported by calculations of the mirror Chern number [see Fig. 3(d)] providing $C_M = -1$. As shown in Fig. 3(e), the nontrivial Chern number protects the presence of 001-surface states even when SOC is included, with a Dirac-like dispersion close to the $\overline{M}$ point.

Further calculations of the strong $\mathbb{Z}_2$ invariant ν show that the J3KM model for the even/odd subspace actually describes a strong $\mathbb{Z}_2$ TI, in agreement with the fact that $\nu \equiv C_M \bmod 2$ [40]. When considering together even and odd layers, the $\mathbb{Z}_2$ invariant of the two subspaces is summed and becomes trivial ($1 + 1 \equiv 0 \bmod 2$), while C_M adds up to -2. On one side, this means that the weak $\mathbb{Z}_2$ topology of bulk jacutingaite does not fit the standard paradigm of weakly coupled QSHI, but it is intimately related to the double band inversion (one for each even/odd subspace) driven by the strong interlayer coupling. On the other, we expect the mirror Chern number to protect the surface states also when both subspaces are considered together.

In order to support this conclusion and at the same time to provide further evidence that the above predictions are not protected by some extra symmetries (e.g., particle-hole) of the simple J3KM model, we finally consider the full MLWF Hamiltonian, which includes in particular additional terms to Eq. (2) that (i) restore the coupling between even and odd layers; (ii) introduce a finite dispersion along the K-H line as in DFT [Fig. 1(c)]; and (iii) break particle-hole symmetry, making the system a compensated semimetal. Still, the topological classification of bulk jacutingaite is not affected. The corresponding band structure for a 60-layer slab is reported in Fig. 3(f). Consistently with $C_M = -2$, two pairs of surface states are present, slightly split by the coupling between even and odd layers. Remarkably, these bands are very similar to what is observed in ARPES experiments [14].

In conclusion, we provide a microscopic insight on how symmetry-protected topological order in layered jacutingaite emerges from a nontrivial coupling between Kane-Mele-type QSHI monolayers. The essential physical features can be captured by a simple generalization of the Kane-Mele model to account for interlayer hopping. This J3KM model predicts the presence of surface states and nodal lines gapped by spin-orbit interactions, in remarkable agreement with recent ARPES measurements and first-principles simulations, providing an appealing strategy to break the standard paradigm of weak topological insulators that becomes relevant for all other layered materials made of stacked honeycomb lattices.

We sincerely acknowledge F. Baumberger, I. Cucchi, and A. Tamai for useful discussions and Ivo Souza for precious comments on the manuscript. This work was supported by the NCCR MARVEL of the Swiss National Science Foundation. M.G. acknowledges support from the Swiss National Science Foundation through the Ambizione program. We also acknowledge support from the European Union's Centre of Excellence MaX "Materials design at the Exascale" (Grant No. 824143). Simulation time was awarded by CSCS on Piz Daint (production Projects s825 and s917) and by PRACE on Marconi at Cineca, Italy (Project id. 2016163963).

[1] F. D. M. Haldane, Model for a Quantum Hall Effect without Landau Levels: Condensed-Matter Realization of the "Parity Anomaly", Phys. Rev. Lett. **61**, 2015 (1988).

[2] K. S. Novoselov, A. K. Geim, S. V. Morozov, D. Jiang, Y. Zhang, S. V. Dubonos, I. V. Grigorieva, and A. A. Firsov, Electric field effect in atomically thin carbon films, Science **306**, 666 (2004).

[3] C. L. Kane and E. J. Mele, Quantum Spin Hall Effect in Graphene, Phys. Rev. Lett. **95**, 226801 (2005).

[4] C. L. Kane and E. J. Mele, $\mathbb{Z}_2$ Topological Order and the Quantum Spin Hall Effect, Phys. Rev. Lett. **95**, 146802 (2005).

[5] B. A. Bernevig and T. L. Hughes, *Topological Insulators and Topological Superconductors* (Princeton University Press, Princeton, NJ, 2013).

[6] A. Molle, J. Goldberger, M. Houssa, Y. Xu, S.-C. Zhang, and D. Akinwande, Buckled two-dimensional Xene sheets, Nat. Mater. **16**, 163 (2017).

[7] C.-C. Liu, W. Feng, and Y. Yao, Quantum Spin Hall Effect in Silicene and Two-Dimensional Germanium, Phys. Rev. Lett. **107**, 076802 (2011).

[8] Y. Xu, B. Yan, H.-J. Zhang, J. Wang, G. Xu, P. Tang, W. Duan, and S.-C. Zhang, Large-Gap Quantum Spin Hall Insulators in Tin Films, Phys. Rev. Lett. **111**, 136804 (2013).

[9] A. Marrazzo, M. Gibertini, D. Campi, N. Mounet, and N. Marzari, Prediction of a Large-Gap and Switchable Kane-Mele Quantum Spin Hall Insulator, Phys. Rev. Lett. **120**, 117701 (2018).

[10] A. R. Cabral, H. F. Galbiatti, R. Kwitko-Ribeiro, and B. Lehmann, Platinum enrichment at low temperatures and related microstructures, with examples of hongshiite (PtCu) and empirical 'Pt_2HgSe_3' from Itabira, Minas Gerais, Brazil, Terra Nova **20**, 32 (2008).

[11] A. Vymazalová, F. Laufek, M. Drábek, A. R. Cabral, J. Haloda, T. Sidorinová, B. Lehmann, H. F. Galbiatti, and J. Drahokoupil, Jacutingaite, Pt_2HgSe_3, a new platinum-group mineral species from the Cauê iron-ore deposit, Itabira district, Minas Gerais, Brazil, Can. Mineral. **50**, 431 (2012).

[12] K. Kandrai, G. Kukucska, P. Vancsó, J. Koltai, G. Baranka, Z. E. Horváth, Á. Hoffmann, A. Vymazalová, L. Tapasztó, and P. Nemes-Incze, Evidence for room temperature quantum spin Hall state in the layered mineral jacutingaite, arXiv:1903.02458.

[13] D. Mauro, H. Henck, M. Gibertini, M. Filippone, E. Giannini, I. Gutierrez-Lezama, and A. F. Morpurgo, Multi-frequency Shubnikov-de Haas oscillations in topological semimetal Pt_2HgSe_3, 2D Materials (2020), doi:10.1088/2053-1583/ab7689.

[14] I. Cucchi, A. Marrazzo, E. Cappelli, S. Riccò, F. Y. Bruno, S. Lisi, M. Hoesch, T. K. Kim, C. Cacho, C. Besnard, E. Giannini, N. Marzari, M. Gibertini, F. Baumberger, and A. Tamai, Bulk and surface electronic structure of the dual-topology semimetal Pt_2HgSe_3, Phys. Rev. Lett. **124**, 106402 (2020).

[15] J. I. Facio, S. K. Das, Y. Zhang, K. Koepernik, J. van den Brink, and I. C. Fulga, Dual topology in jacutingaite Pt_2HgSe_3, Phys. Rev. Mater. **3**, 074202 (2019).

[16] B. Ghosh, S. Mardanya, B. Singh, X. Zhou, B. Wang, T.-R. Chang, C. Su, H. Lin, A. Agarwal, and A. Bansil, Saddle-point Van Hove singularity and dual topological state in Pt_2HgSe_3, Phys. Rev. B **100**, 235101 (2019).

[17] X. Wu, M. Fink, W. Hanke, R. Thomale, and D. Di Sante, Unconventional superconductivity in a doped quantum spin Hall insulator, Phys. Rev. B **100**, 041117(R) (2019).

[18] M. Z. Hasan and C. L. Kane, *Colloquium*: Topological insulators, Rev. Mod. Phys. **82**, 3045 (2010).

[19] T. Rauch, M. Flieger, J. Henk, I. Mertig, and A. Ernst, Dual Topological Character of Chalcogenides: Theory for Bi_2Te_3, Phys. Rev. Lett. **112**, 016802 (2014).

[20] M. Eschbach, M. Lanius, C. Niu, E. Młyńczak, P. Gospodarič, J. Kellner, P. Schüffelgen, M. Gehlmann, S. Döring, E. Neumann, M. Luysberg, G. Mussler, L. Plucinski, M. Morgenstern, D. Grützmacher, G. Bihlmayer, S. Blügel, and C. M. Schneider, Bi_1Te_1 is a dual topological insulator, Nat. Commun. **8**, 14976 EP (2017).

[21] N. Marzari, A. A. Mostofi, J. R. Yates, I. Souza, and D. Vanderbilt, Maximally localized wannier functions: Theory and applications, Rev. Mod. Phys. **84**, 1419 (2012).

[22] C.-C. Liu, H. Jiang, and Y. Yao, Low-energy effective hamiltonian involving spin-orbit coupling in silicene and two-dimensional germanium and tin, Phys. Rev. B **84**, 195430 (2011).

[23] $v_{ij} = \pm 1$ depending on the orientation of the two NN bonds $\boldsymbol{d}_{1,2}$ (and can be written as $\boldsymbol{d}_1 \times \boldsymbol{d}_2/|\boldsymbol{d}_1 \times \boldsymbol{d}_2|$), $u_{ij} = \pm 1$ for the two sublattices and $\boldsymbol{d}^0_{ij}$ is the unit vector connecting two second-nearest neighbors.

[24] See Supplemental Material at http://link.aps.org/supplemental/10.1103/PhysRevResearch.2.012063 for details of the first-principles calculations and of the 3D Kane-Mele model and its connections with the SSH model.

[25] N. Mounet, M. Gibertini, P. Schwaller, D. Campi, A. Merkys, A. Marrazzo, T. Sohier, I. E. Castelli, A. Cepellotti, G. Pizzi, and N. Marzari, Two-dimensional materials from high-throughput computational exfoliation of experimentally known compounds, Nat. Nanotechnol. **13**, 246 (2018).

[26] R. Yu, X. L. Qi, A. Bernevig, Z. Fang, and X. Dai, Equivalent expression of $\mathbb{Z}_2$ topological invariant for band insulators using the non-Abelian Berry connection, Phys. Rev. B **84**, 075119 (2011).

[27] The J3KM model without SOC displays an extra chiral symmetry that constrains surface states to be at $E = 0$, although it is not necessary for their existence.

[28] J. Zak, Berry's Phase for Energy Bands in Solids, Phys. Rev. Lett. **62**, 2747 (1989).

[29] D. Vanderbilt, *Berry Phases in Electronic Structure Theory* (Cambridge University Press, Cambridge, 2018).

[30] W. A. Benalcazar, B. A. Bernevig, and T. L. Hughes, Electric multipole moments, topological multipole moment pumping, and chiral hinge states in crystalline insulators, Phys. Rev. B **96**, 245115 (2017).

[31] C.-K. Chiu, Y.-H. Chan, and A. P. Schnyder, Quantized Berry Phase and Surface States under Reflection Symmetry or Space-Time Inversion Symmetry, arXiv:1810.04094.

[32] The relationship between nodal lines and Zak (or Berry) phases is a general feature of systems with time reversal and inversion symmetry [33–37] that goes beyond the applicability of the SSH analogy.

[33] R. Yu, H. Weng, Z. Fang, X. Dai, and X. Hu, Topological Node-Line Semimetal and Dirac Semimetal State in Antiperovskite Cu_3PdN, Phys. Rev. Lett. **115**, 036807 (2015).

[34] Y. Kim, B. J. Wieder, C. L. Kane, and A. M. Rappe, Dirac Line Nodes in Inversion-Symmetric Crystals, Phys. Rev. Lett. **115**, 036806 (2015).

[35] C. Fang, Y. Chen, H.-Y. Kee, and L. Fu, Topological nodal line semimetals with and without spin-orbital coupling, Phys. Rev. B **92**, 081201(R) (2015).

[36] Y.-H. Chan, C.-K. Chiu, M. Y. Chou, and A. P. Schnyder, Ca_3P_2 and other topological semimetals with line nodes and drumhead surface states, Phys. Rev. B **93**, 205132 (2016).

[37] C. Fang, H. Weng, X. Dai, and Z. Fang, Topological nodal line semimetals, Chin. Phys. B **25**, 117106 (2016).

[38] The peculiar nature of $\tilde{H}_{2^{\rm nd}{\rm NL}}$ allows the transition to happen at relatively small interlayer coupling (and thus realistic in layered materials), differently from other intrinsically 3D models describing the transition between weak and strong topological phases [39].

[39] L. Fu, C. L. Kane, and E. J. Mele, Topological Insulators in Three Dimensions, Phys. Rev. Lett. **98**, 106803 (2007).

[40] D. Varjas, F. de Juan, and Y.-M. Lu, Bulk invariants and topological response in insulators and superconductors with nonsymmorphic symmetries, Phys. Rev. B **92**, 195116 (2015).

Supplemental Material for "*Emergent dual topology in the three-dimensional Kane-Mele Pt_2HgSe_3*"

Antimo Marrazzo,[1] Nicola Marzari,[1] and Marco Gibertini[2]

[1] *Theory and Simulation of Materials (THEOS), and National Centre for Computational Design and Discovery of Novel Materials (MARVEL), École Polytechnique Fédérale de Lausanne, CH-1015 Lausanne, Switzerland*

[2] *Department of Quantum Matter Physics, University of Geneva, 24 Quai Ernest Ansermet, CH-1211 Geneva, Switzerland*

(Dated: December 5, 2019)

S1. FIRST-PRINCIPLES SIMULATIONS

Density-functional theory calculations are performed with the Quantum ESPRESSO distribution [1, 2], Wannier functions are obtained using WANNIER90 [3]. Structural optimization is performed by using the experimental lattice parameters as obtained from X-ray diffraction and relaxing the atomic coordinates with a non-local van der Waals functional, namely the vdW-DF2 functional [4] with C09 exchange (DF2-C09) [5], and the SSSP precision pseudopotential library v1.0 [6] with 100 Ry of wavefunction cutoff and a dual of 8. Further calculations on the optimized crystal structure (band structures and Wannier functions) are performed using the PBE functional [7] and ONCV [8] scalar and fully relativistic pseudopotentials from the PseudoDojo library [9] with 80 Ry of wavefunction cutoff and a dual of 4. All calculation are perfomed with $\mathbf{k}$-point density of 0.09 Å^{-1}, that corresponds to a $\mathbf{k}-$point grid of $12 \times 12 \times 14$, and Marzari-Vanderbilt smearing [10] of 0.015 Ry. Wannier functions are constructed from a $\mathbf{k}-$point grid of $6\times6\times6$. Part of the calculations are powered by the AiiDA [11] materials' informatics infrastructure.

S2. 4-BAND MODEL FOR BULK JACUTINGAITE

In order to construct a minimal tight-binding model for bulk jacutingaite, we follow a similar strategy as for the monolayer [12] by mapping first-principles calculations onto a set of maximally-localized Wannier functions (MLWFs) [13], constructed from an initial projection on Hg-centred s-like orbitals. This results in a 4-band (including spin and relativistic effects) tight-binding model on a lattice made of buckled honeycomb layers directly stacked on top of each other (AA stacking). We denote the lattice vectors of the unit cell with $\boldsymbol{a}_1 = (a, 0, 0)$, $\boldsymbol{a}_2 = (-a/2, \sqrt{3}a/2, 0)$, and $\boldsymbol{a}_3 = (0, 0, c)$, with the two inequivalent sublattices centered at $\boldsymbol{\tau}_A = 2/3\boldsymbol{a}_1+1/3\boldsymbol{a}_2+\delta\boldsymbol{a}_3$ and $\boldsymbol{\tau}_B = 1/3\boldsymbol{a}_1+2/3\boldsymbol{a}_2-\delta\boldsymbol{a}_3$. The band structure obtained from this 4-band model is compared to the original first-principles results in Fig. S1. Although a perfect quantitative agreement is not attainable, the model reproduces all qualitative features around the Fermi energy, including in particular the extended linear dispersion and the very small band gap between valence and conduction bands at K and H.

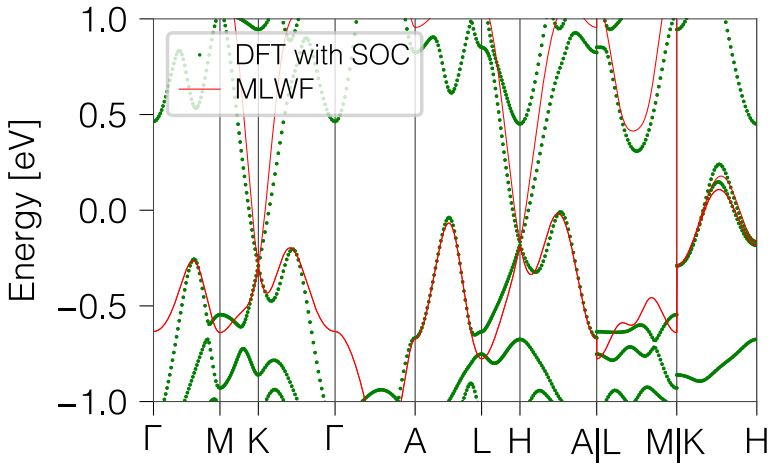

FIG. S1. Band structure of bulk jacutingaite along a high-symmetry path as obtained from first-principles calculations (green dots) and from the MLWF 4-band model (red line).

S3. SECOND-NEAREST-LAYER HOPPING TERM

Within the 4-band model, the largest hopping term involves MLWFs that are centered on neighboring sites in the same layer, with amplitude $t = 0.27$ eV. As mentioned in the main text, the next largest contribution is a second-nearest layer hopping term with amplitude $t_2 = -0.18$ eV $\simeq -0.7\ t$. This hopping process involves a reference Wannier function on the A (B) sublattice and one of three B (A) sites that lie 2 layers above (below) in unit cells identified by the lattice vectors

$$\boldsymbol{R}_1 = \pm(\boldsymbol{a}_1 - \boldsymbol{a}_2 + 2\boldsymbol{a}_3), \quad \boldsymbol{R}_2 = \pm(-\boldsymbol{a}_1 - \boldsymbol{a}_2 + 2\boldsymbol{a}_3), \quad \boldsymbol{R}_3 = \pm(\boldsymbol{a}_1 + \boldsymbol{a}_2 + 2\boldsymbol{a}_3). \tag{S1}$$

In Fig. S2 we sketch the sites involved in this hopping process, starting either from the A sublattice (red solid arrows, upper signs in Eq. (S1)) or the B sublattice (blue dashed arrows, lower signs in Eq. (S1)). This hopping term has been adopted in the main text to construct a minimal extension of the 2D Kane-Mele model that is able to describe the emergent topology in bulk jacutingaite.

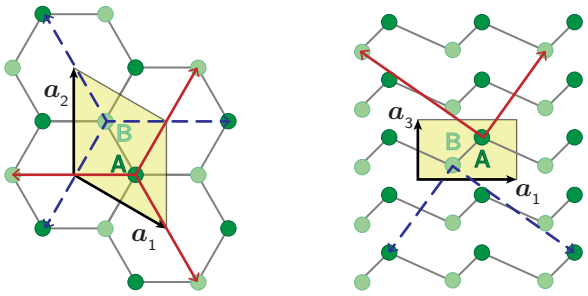

FIG. S2. Schematic representation of the buckled honeycomb lattice formed by Hg atoms on which the 4-band MLWF tight-binding model is defined. The A (B) sublattice is denoted with dark (light) green circles. The shaded yellow area shows the primitive unit cell, with lattice vectors $\boldsymbol{a}_1$, $\boldsymbol{a}_2$, and $\boldsymbol{a}_3$. Arrows connect sites involved in the second-nearest layer hopping process responsible for the non-trivial topological properties of bulk jacutingaite, starting from either the A sublattice (red solid arrows, corresponding to the vectors $\boldsymbol{\tau}_B + \boldsymbol{R}_{1,2,3} - \boldsymbol{\tau}_A$ with the upper sign in Eq. (S1)) or the B sublattice (blue dashed arrows, corresponding to the vectors $\boldsymbol{\tau}_A + \boldsymbol{R}_{1,2,3} - \boldsymbol{\tau}_B$ with the lower sign in Eq. (S1)).

S4. CONNECTION WITH THE SU-SCHRIEFFER-HEEGER MODEL

In the absence of spin-orbit coupling, the J3KM model reduces to a 2-band model with a corresponding 2×2 Hamiltonian in Fourier space that can be written

$$\mathcal{H}(\boldsymbol{k}_\parallel, k_z) = \begin{pmatrix} 0 & tf(\boldsymbol{k}_\parallel) + t_2 g(\boldsymbol{k}_\parallel) e^{i2k_z c} \\ tf^*(\boldsymbol{k}_\parallel) + t_2 g^*(\boldsymbol{k}_\parallel) e^{-i2k_z c} & 0 \end{pmatrix} \tag{S2}$$

where $\boldsymbol{k}_\parallel = (k_x, k_y)$ and according to Sec. S3 we have

$$f(\boldsymbol{k}_\parallel) = 1 + e^{i\boldsymbol{k}_\parallel \cdot \boldsymbol{a}_1} + e^{-i\boldsymbol{k}_\parallel \cdot \boldsymbol{a}_2} = e^{i(k_x - \sqrt{3}k_y)a/2} \left[1 + 2e^{i\sqrt{3}k_y a/2} \cos\left(\frac{k_x a}{2}\right) \right] \tag{S3}$$

$$g(\boldsymbol{k}_\parallel) = e^{i\boldsymbol{k}_\parallel \cdot (\boldsymbol{a}_1 + \boldsymbol{a}_2)} + e^{i\boldsymbol{k}_\parallel \cdot (\boldsymbol{a}_1 - \boldsymbol{a}_2)} + e^{-i\boldsymbol{k}_\parallel \cdot (\boldsymbol{a}_1 + \boldsymbol{a}_2)} = e^{i\boldsymbol{k}_\parallel \cdot (\boldsymbol{a}_1 - \boldsymbol{a}_2)} f^*(2\boldsymbol{k}_\parallel) = e^{i(k_x - \sqrt{3}k_y)a/2} \left[e^{i\sqrt{3}k_y a} + 2\cos(k_x a) \right] \tag{S4}$$

If we now write $f(\boldsymbol{k}_\parallel) = |f(\boldsymbol{k}_\parallel)| e^{i\phi(\boldsymbol{k}_\parallel)}$, we thus have that $g(\boldsymbol{k}_\parallel) = |f(2\boldsymbol{k}_\parallel)| e^{-i\phi(2\boldsymbol{k}_\parallel) + i\boldsymbol{k}_\parallel \cdot (\boldsymbol{a}_1 - \boldsymbol{a}_2)}$ and the Hamiltonian can be written as

$$\begin{aligned} \mathcal{H}(\boldsymbol{k}_\parallel, k_z) &= \begin{pmatrix} 0 & t|f(\boldsymbol{k}_\parallel)| e^{i\phi(\boldsymbol{k}_\parallel)} + t_2 |f(2\boldsymbol{k}_\parallel)| e^{i2k_z c - i\phi(2\boldsymbol{k}_\parallel) + i\boldsymbol{k}_\parallel \cdot (\boldsymbol{a}_1 - \boldsymbol{a}_2)} \\ t|f(\boldsymbol{k}_\parallel)| e^{-i\phi(\boldsymbol{k}_\parallel)} + t_2 |f(2\boldsymbol{k}_\parallel)| e^{-i2k_z c + i\phi(2\boldsymbol{k}_\parallel) - i\boldsymbol{k}_\parallel \cdot (\boldsymbol{a}_1 - \boldsymbol{a}_2)} & 0 \end{pmatrix} \\ &= \begin{pmatrix} 1 & 0 \\ 0 & e^{-i\phi(\boldsymbol{k}_\parallel)} \end{pmatrix} \begin{pmatrix} 0 & t|f(\boldsymbol{k}_\parallel)| + t_2 |f(2\boldsymbol{k}_\parallel)| e^{i[2k_z c - \alpha(\boldsymbol{k}_\parallel)]} \\ t|f(\boldsymbol{k}_\parallel)| + t_2 |f(2\boldsymbol{k}_\parallel)| e^{-i[2k_z c - \alpha(\boldsymbol{k}_\parallel)]} & 0 \end{pmatrix} \begin{pmatrix} 1 & 0 \\ 0 & e^{i\phi(\boldsymbol{k}_\parallel)} \end{pmatrix} \end{aligned} \tag{S5}$$

where $\alpha(\boldsymbol{k}_\parallel) = \big[\phi(\boldsymbol{k}_\parallel) + \phi(2\boldsymbol{k}_\parallel) - \boldsymbol{k}_\parallel \cdot (\boldsymbol{a}_1 - \boldsymbol{a}_2)\big]$. This is Hamiltonian is unitarily equivalent to the Hamiltonian of the Su-Schriffer-Heger (SSH) model, where the hopping energies depend parametrically on the in-plane wave vector $\boldsymbol{k}_\parallel$ and the effect of the extra phase $\alpha(\boldsymbol{k}_\parallel)$ in one of the hopping amplitudes is simply to shift the dispersion of the energy bands as a function of k_z for a given value of $\boldsymbol{k}_\parallel$. The effective SSH hopping amplitudes become

$$\tilde{t}(\boldsymbol{k}_\parallel) = t|f(\boldsymbol{k}_\parallel)| \qquad \text{and} \qquad \tilde{t}_2(\boldsymbol{k}_\parallel) = t_2|f(2\boldsymbol{k}_\parallel)|e^{-i\alpha(\boldsymbol{k}_\parallel)} \ . \tag{S6}$$

The condition for the gap to close reads $|\tilde{t}(\boldsymbol{k}_\parallel)| = |\tilde{t}_2(\boldsymbol{k}_\parallel)|$, which has non-trivial solutions only when $|t_2/t| > 1/3$. At the values of $\boldsymbol{k}_\parallel$ for which this condition is satisfied there must exist a value of k_z (which depends on $\alpha(\boldsymbol{k}_\parallel)$) at which the gap closes, thus giving rise to a nodal line. We have verified that, as expected, the projection of the nodal line on the (k_x, k_y)-plane (as identified by the solution of $|\tilde{t}(\boldsymbol{k}_\parallel)| = |\tilde{t}_2(\boldsymbol{k}_\parallel)|$) coincides with the line separating regions where the Zak phase (computed from the eigenstates of (S2)) is trivial and regions where it is non-trivial.

[1] P. Giannozzi, S. Baroni, N. Bonini, M. Calandra, R. Car, C. Cavazzoni, Davide Ceresoli, G. L. Chiarotti, M. Cococcioni, I. Dabo, A. D. Corso, S. de Gironcoli, S. Fabris, G. Fratesi, R. Gebauer, U. Gerstmann, C. Gougoussis, Anton Kokalj, M. Lazzeri, L. Martin-Samos, N. Marzari, F. Mauri, R. Mazzarello, Stefano Paolini, A. Pasquarello, L. Paulatto, C. Sbraccia, S. Scandolo, G. Sclauzero, A. P. Seitsonen, A. Smogunov, P. Umari, and R. M. Wentzcovitch, *QUANTUM ESPRESSO: A Modular and Open-Source Software Project for Quantum Simulations of Materials*, Journal of Physics: Condensed Matter **21**, 395502 (2009).

[2] P. Giannozzi, O. Andreussi, T. Brumme, O. Bunau, M. B. Nardelli, M. Calandra, R. Car, C. Cavazzoni, D Ceresoli, M. Cococcioni, N. Colonna, I. Carnimeo, A. D. Corso, S. de Gironcoli, P. Delugas, R. A. D. Jr, A Ferretti, A. Floris, G. Fratesi, G. Fugallo, R. Gebauer, U. Gerstmann, F. Giustino, T. Gorni, J. Jia, M. Kawamura, H-Y Ko, A. Kokalj, E. Küçükbenli, M. Lazzeri, M. Marsili, N. Marzari, F. Mauri, N. L. Nguyen, H.-V. Nguyen, A Otero-de-la-Roza, L. Paulatto, S. Poncé, D. Rocca, R. Sabatini, B. Santra, M. Schlipf, A. P. Seitsonen, A. Smogunov, I Timrov, T. Thonhauser, P. Umari, N. Vast, X. Wu, and S. Baroni, *Advanced Capabilities for Materials Modelling with Q Uantum ESPRESSO*, Journal of Physics: Condensed Matter **29**, 465901 (2017).

[3] A. A. Mostofi, J. R. Yates, G. Pizzi, Y.-S. Lee, I. Souza, D. Vanderbilt, and N. Marzari, *An Updated Version of Wannier90: A Tool for Obtaining Maximally-Localised Wannier Functions*, Computer Physics Communications **185**, 2309 (2014).

[4] K. Lee, É. D. Murray, L. Kong, B. I. Lundqvist, and D. C. Langreth, *Higher-Accuracy van Der Waals Density Functional*, Physical Review B **82**, 081101 (2010).

[5] V. R. Cooper, *Van Der Waals Density Functional: An Appropriate Exchange Functional*, Physical Review B **81**, 161104 (2010).

[6] G. Prandini, A. Marrazzo, I. E. Castelli, N. Mounet, and N. Marzari, *Precision and efficiency in solid-state pseudopotential calculations*, npj Computational Materials **4**, 72 (2018).

[7] J. P. Perdew, K. Burke, and M. Ernzerhof, *Generalized Gradient Approximation Made Simple*, Physical Review Letters **77**, 3865 (1996).

[8] D. R. Hamann, *Optimized Norm-Conserving Vanderbilt Pseudopotentials*, Physical Review B **88**, 085117 (2013).

[9] M. J. van Setten, M. Giantomassi, E. Bousquet, M. J. Verstraete, D. R. Hamann, X. Gonze, and G. M. Rignanese, *The PseudoDojo: Training and grading a 85 element optimized norm-conserving pseudopotential table*, Computer Physics Communications **226**, 39 (2018).

[10] N. Marzari, D. Vanderbilt, A. De Vita, and M. C. Payne, *Thermal Contraction and Disordering of the Al(110) Surface*, Phys. Rev. Lett. **82**, 3296 (1999).

[11] G. Pizzi, A. Cepellotti, R. Sabatini, N. Marzari, and B. Kozinsky, *AiiDA: Automated Interactive Infrastructure and Database for Computational Science*, Computational Materials Science **111**, 218 (2016).

[12] A. Marrazzo, M. Gibertini, D. Campi, N. Mounet, and N. Marzari, *Prediction of a Large-Gap and Switchable Kane-Mele Quantum Spin Hall Insulator*, Phys. Rev. Lett. **120**, 117701 (2018).

[13] N. Marzari, A. A. Mostofi, J. R. Yates, I. Souza, and D. Vanderbilt, *Maximally Localized Wannier Functions: Theory and Applications*, Reviews of Modern Physics **84**, 1419 (2012).